

Accelerated Publications

A New Pathway for Transmembrane Electron Transfer in Photosynthetic Reaction Centers of *Rhodobacter sphaeroides* Not Involving the Excited Special Pair[†]

Marion E. Van Brederode,^{*,‡} Michael R. Jones,[§] Frank Van Mourik,[‡] Ivo H. M. Van Stokkum,[‡] and Rienk Van Grondelle[‡]

Department of Physics and Astronomy, Free University of Amsterdam, De Boelelaan 1081, 1081 HV, Amsterdam, The Netherlands, and Krebs Institute for Biomolecular Research and Robert Hill Institute for Photosynthesis, Department of Molecular Biology and Biotechnology, University of Sheffield, Western Bank, Sheffield, S10 2UH, United Kingdom

Received February 19, 1997; Revised Manuscript Received April 29, 1997[⊗]

ABSTRACT: It is generally accepted that electron transfer in bacterial photosynthesis is driven by the first singlet excited state of a special pair of bacteriochlorophylls (P^{*}). We have examined the first steps of electron transfer in a mutant of the *Rhodobacter sphaeroides* reaction center in which charge separation from P^{*} is dramatically slowed down. The results provide for the first time clear evidence that excitation of the monomeric bacteriochlorophyll in the active branch of the reaction center (B_A) drives ultrafast transmembrane electron transfer without the involvement of P^{*}, demonstrating a new and efficient mechanism for solar energy transduction in photosynthesis. The most abundant charge-separated intermediate state probably is P⁺B_A⁻, which is formed within 200 fs from B_A^{*} and decays with a lifetime of 6.5 ps into P⁺H_A⁻. We also see evidence for the involvement of a B_A⁺H_A⁻ state in the alternative pathway.

In photosynthesis, the conversion of light energy into electrochemical energy takes place in membrane-spanning pigment–protein complexes termed reaction centers (RCs).¹ In *Rhodobacter (Rb.) sphaeroides*, a purple photosynthetic bacterium, the excitation of one of the pigments of the bacterial RC gives rise to a sequence of electron transfer

reactions selectively along one of the two near-symmetric branches of cofactors (see Figure 1). It is clear that this energy transduction process involves the transfer of an electron from a pair of bacteriochlorophyll molecules (the primary donor, P) located on one side of the membrane to a molecule of ubiquinone located on the opposite side of the membrane. The general features of this picosecond (ps) process have been well established through the application of time-resolved measurements (1–3). It is widely accepted that upon excitation of any of the four “monomeric” pigments (B_A, B_B, H_A, and H_B in Figure 1) all excited state energy is funnelled downhill to P in approximately 100 femtoseconds (fs), leading to the formation of state P^{*} (4–6). This P^{*} state then drives charge separation to the bacteriopheophytin molecule (H_A), most probably via the monomeric bacteriochlorophyll molecule (B_A), in approximately 3.5 ps. This is followed by electron transfer from H_A to the Q_A quinone, creating the radical pair state P⁺Q_A⁻ (1, 2, 3).

[†] This research is supported by the Dutch Foundation for Fundamental Research (NWO) through the foundation for Life Sciences (SLW) and EC Contract CT930278. M.R.J. is a Biotechnology and Biological Sciences Research Council Advanced Research Fellow.

* Correspondence should be addressed to this author at the Free University of Amsterdam, De Boelelaan 1081, 1081 HV Amsterdam, The Netherlands. Fax: 31-20-4447999. E-mail: marion@nat.vu.nl.

[‡] Free University of Amsterdam.

[§] University of Sheffield.

[⊗] Abstract published in *Advance ACS Abstracts*, June 1, 1997.

¹ Abbreviations: RC(s); reaction centers; WT, wild-type; P, primary donor; H, bacteriopheophytin; B, monomeric bacteriochlorophyll; Q, quinone; *Rb.*, *Rhodobacter*; SADS, species-associated difference spectrum.

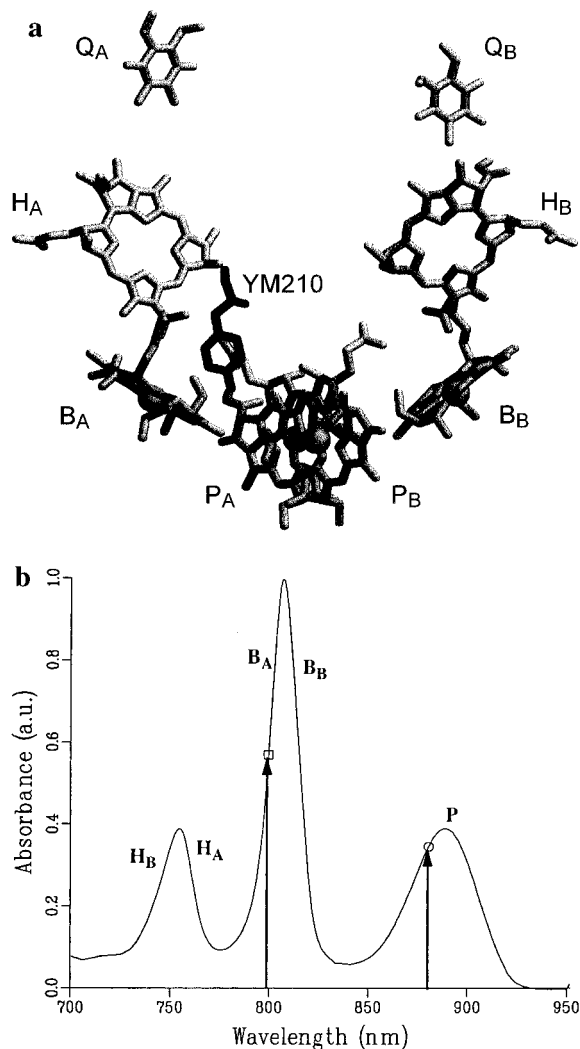


FIGURE 1: (A) Schematic of the arrangement of the cofactors present in the *Rb. sphaeroides* RC. The structure of the complex has been solved to high resolution by X-ray crystallography (28, 29). Four bacteriochlorophylls (P_A, P_B, B_A, B_B), two bacteriopheophytins (H_A, H_B), and two ubiquinones (Q_A, Q_B) are arranged in two near-symmetrical branches that span the membrane. For clarity, the phytol tails of the cofactors have been omitted. The remaining cofactors are a molecule of carotenoid and a non-heme iron atom (not shown). The position of tyrosine (Y) M210 in the structure of the wild-type RC is also shown. In the experiments presented here, this residue was mutated to tryptophan, as described previously (15). (B) 77K absorption spectrum of RC-only membranes from the YM210W mutant. The approximate positions of the Q_y absorption bands of these cofactors are indicated, as are the wavelengths of laser excitation used in this study.

Recently, we have concluded that the pigments present in the active branch of the RC, i.e., H_A and B_A, are only partially effective in transferring their energy to P at cryogenic temperature (77 K) in a mutated *Rb. sphaeroides* RC (YM210W) (7). This conclusion was based upon measurements of the excitation spectrum of the steady-state fluorescence emission from P* in this RC. The contributions of B_A and H_A were largely absent from the excitation spectrum. However, the action spectrum of P⁺Q_A⁻ formation demonstrated that the excited state energy that was not transferred from B_A* and H_A* to P was still effective in driving electron transfer. The implication of these findings was that an alternative route of transmembrane electron transfer may exist in this mutant which involves B_A* and H_A*, and which bypasses P*. Electron transfer from P* to P⁺H_A⁻

at 77 K in membrane-bound YM210W RCs is extremely slow and is associated with a time constant for P* decay of ~400 ps (8, 15) as compared to 2 ps in wild-type (WT) RCs (9). The reasons for the slow electron transfer in this, and related mutants, have been discussed in detail elsewhere (10–16). The general view is that the free energy of the state P⁺B_A⁻ has been raised in the slow M210 mutants, such as YM210W, thereby making the first electron transfer event energetically less favorable (13, 16, 17). The decrease in the primary electron transfer rate results in a diminishing of the efficiency of P⁺Q_A⁻ formation to 80% at room temperature and 60% at cryogenic temperatures, relative to WT RCs (8). For RCs in which Q_A is reduced, the quantum yield for P⁺H_A⁻ formation is between 25 and 50% (8, 15). Any alternative route for electron transfer from B_A* must start with a process that occurs on a subpicosecond time scale, if the route is to compete with the ~100 fs energy transfer from B_A* to P (4–6). In this work, we have investigated membrane-bound YM210W RCs in detail using ultrafast laser spectroscopy. By comparing the effects of direct excitation of P at 880 nm, with excitation of the B_A monomeric bacteriochlorophyll at 799 nm, we have established that an alternative route for charge separation indeed exists in this mutant.

MATERIALS AND METHODS

Sample Preparation. The construction of the mutant RC bearing the change YM210 → W has been described previously (16). The mutated RC genes were expressed in a strain of *Rb. sphaeroides* that lacks the genes for the LH1 and LH2 antenna complexes, producing a strain which had an antenna-deficient, RC-only phenotype (30). The experimental material was intracytoplasmic membranes prepared from cells of the RC-only mutant strain (31). The RC-only membranes were mixed with ~70% glycerol containing 25 mM potassium phosphate, pH 7.8. Experiments were performed in 1 and 3 mm cuvettes. The OD of the RC-only membranes in the maximum of the ~806 nm absorption band was approximately 0.9 for both types of cuvettes.

Laser System. The experimental system consisted of a laser spectrometer as described in (21). The 799 and 880 nm excitation pulses were selected from a white light continuum using interference filters and were amplified in two dye cells (Styryl 9M and LDS 867, for 799 and 880 nm pulses, respectively). The repetition frequency of the laser system was 30 Hz, which was sufficiently slow to avoid accumulation of the YM210W RCs in the P⁺Q_A⁻ state [which recombines to the ground state in less than 20 ms at 77K (8)]. The 799 nm excitation pulse had a full width at half-maximum (FWHM) of 10 nm, and predominantly excited the active branch monomeric bacteriochlorophyll B_A. The 880 nm excitation pulse had a FWHM of 20 nm, and directly excited P. All spectra were recorded using probe light at magic angle relative to the vertically polarized excitation light. For the various measurements, the excitation energy at the sample was between 1 and 1.5 μJ per pulse, and the diameter of the spot illuminated by the excitation pulse was 300 μm. At this excitation density, between 10 and 20% of the RCs were bleached.

About 250 shots were averaged per delay position both with and without the excitation light on the sample. Each dataset consisted of a total of 41 or 67 time-gated spectra

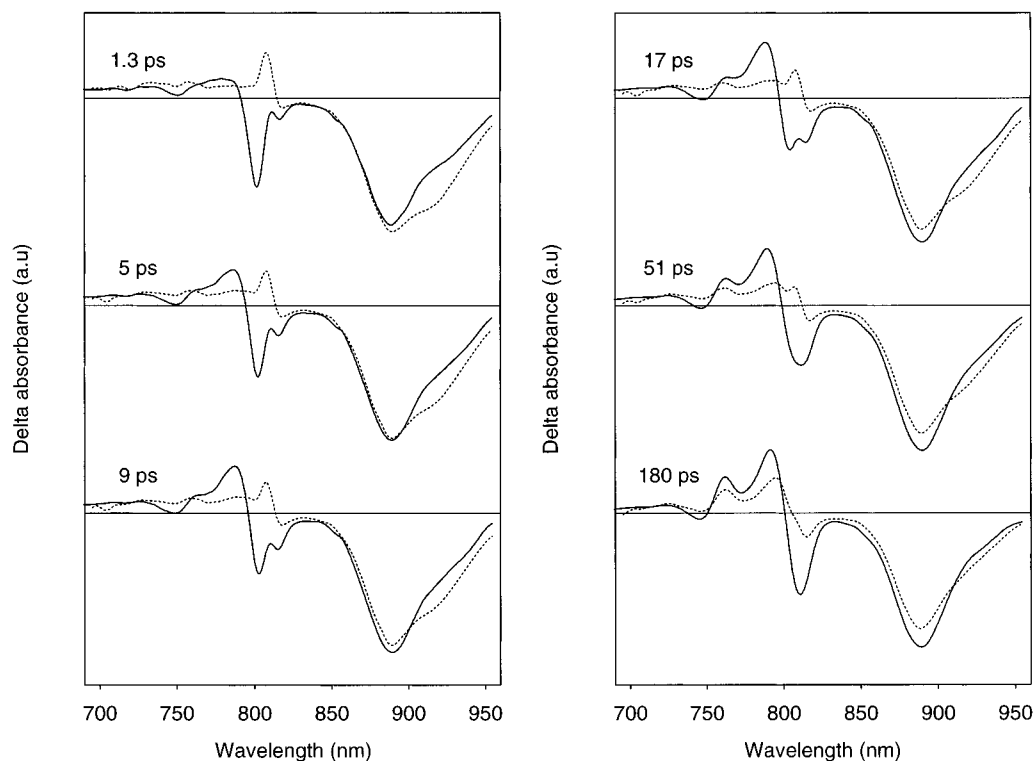


FIGURE 2: Transient absorbance difference spectra obtained at 1.3 ps, 5 ps, 9 ps, 17 ps, 51 ps, and 180 ps after a ~ 190 fs (FWHM) excitation pulse centered at 799 nm (solid spectra) or at 880 nm (dotted spectra). The spectra are reconstructed from the global analysis.

measured up to a maximum of 305 ps after the excitation pulse. Datasets were collected over four different wavelength windows for 799 nm excitation (725–855 nm, 775–905 nm, 825–955 nm, 645–775 nm) and three wavelength windows (700–830 nm, 755–885 nm, 820–950 nm) for 880 nm excitation. In each wavelength window, 3–7 time series of spectra were collected. When the fitted position of time zero, which equals the maximum of the instrument response function, for these datasets was identical within 30 fs, the datasets were averaged before further analysis. The group velocity dispersion was tuned to be optimal by changing the amount of prism in the probe pathway and measuring the CS₂ birefringence signal between two crossed polarizers. The group velocity dispersion (GVD) varied for the different 130 nm wavelength windows between -5 and 5 fs/nm, resulting in a maximum dispersion of about 300 fs relative to time zero for the outer wavelength windows. The instrument response function of the setup determined from the CS₂ signal was 420 fs FWHM. The instrument response resulting from the analysis of the data over all wavelength windows was identical to this value within 15%.

Data Analysis. The datasets obtained with the same excitation wavelength were analyzed simultaneously with linked kinetics and instrument response function using the method of global analysis with an irreversible sequential model with four or five increasing lifetimes (13, 16, 22). The amplitude and spectral shape of each species-associated difference spectrum (SADS) and the position of time zero were not linked. The magic angle P⁺Q_A⁻ difference spectrum measured with double lock-in detection (8) was added as an extra spectrum at a time delay of 10 ns, since the last measured spectrum at 305 ps still contained a considerable amount of P^{*}-stimulated emission for both the 799 nm excitation and the 880 nm excitation datasets. Not doing this revealed one time constant less together with a

decrease of the value of the largest time constant. The scaling of the P⁺Q_A⁻ spectrum was chosen such that the three latest spectra were fitted optimally. The slowest time constants depend somewhat on the scaling of this end spectrum. The datasets, which were sometimes measured on different days and with a slightly different excitation density and sample concentration, were scaled such that the overlapping wavelength regions had the same amplitude. After this scaling, the SADS of the different datasets overlapped very well. The spectra in Figure 2 and 3 are smoothed averages of the fitted results of the overlapping datasets.

RESULTS AND DISCUSSION

In Figure 2 we show absorption difference spectra of the YM210W membrane-bound RC at 77 K for various time delays after excitation of B_A and partial excitation of B_B at 799 nm. At each point in time, the spectra are compared with those obtained following direct excitation of P at 880 nm. If it were the case that, as is generally assumed, all excitation energy residing on B^{*} is transferred on a subpicosecond time scale to P, then the two sets of spectra should have looked very similar; i.e., after a few hundred femtoseconds, the spectral evolution in the YM210W mutant should be insensitive to the wavelength of excitation. This clearly was not the case. The spectra obtained with direct excitation of P are entirely consistent with a slow evolution of the P^{*} state to the P⁺Q_A⁻ radical pair (Figure 2, dotted curves). At time delays of 1.3, 5, 9, and 17 ps after the 880 nm excitation pulse, only P^{*} contributes to the time-gated spectra: there is a strong negative feature from 860 to 950 nm due to the bleaching of the P ground state absorbance band and the presence of P^{*}-stimulated emission. At 808 nm, there is a positive feature which is also characteristic for P^{*} (1). Only at later times (51 and 180 ps dotted in

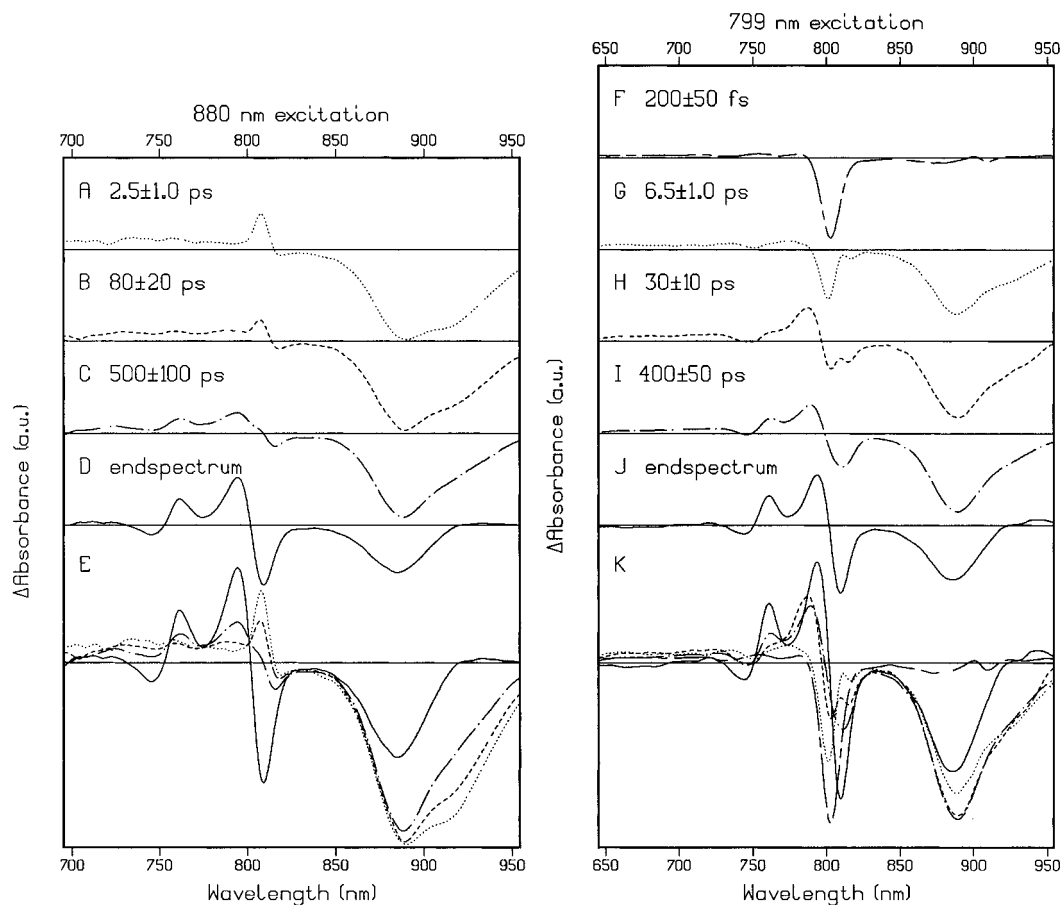


FIGURE 3: Results of a global analysis using a sequential model with four or five increasing lifetimes (i.e., $1 \rightarrow 2 \rightarrow 3 \rightarrow 4 \rightarrow 5$) of transient absorbance difference spectra of the YM210W RC-only membranes obtained after 880 nm (A–D) and 799 nm (F–J) excitation. The lifetimes of the SADS are depicted in the figures. Panels E and K depict an overlay of spectra A–D and F–J, respectively. For comparison, spectrum F has been multiplied by a factor of 0.2.

Figure 2), spectral characteristics for charge separation start to be observed, i.e., the formation of bandshift and bleaching signals in the B and H absorbance region. In contrast, direct excitation of B_A at 799 nm results in difference spectra that contain contributions from B and H, even on a short time scale (Figure 2, solid curves). The spectrum at 1.3 ps shows a very strong bleach of the B absorbance band, and there is a bleach in the H absorbance region superimposed on the excited state absorbance (see also Figure 4). Also stimulated emission and P absorbance bleaching are observed in the spectrum at 1.3 ps, indicating that also energy transfer from B^* to P^* has occurred. However, in comparison with the P band excitation experiment, the amount of stimulated emission is much lower after excitation of the B band at 799 nm, indicating that part of the bleaching does not arise from the formation of P^* , but rather from another state involving P, most likely P^+ . At 9 and 17 ps, the bleaching in the B absorbance region has changed to a spectrum with an electrochromic bandshift that is characteristic for the formation of $P^+H_A^-$. At these times, the P absorbance bleaching signal has also further increased compared to the signal at 1.3 ps, indicating that in the spectrum after 1.3 ps a fraction of radical pairs was present that did not involve P and that during a time scale of 3–15 ps led to the formation of some additional P^+ .

The time constants associated with the spectral changes described in Figure 2 were obtained from a global analysis of the full set of time-resolved difference spectra, using an irreversible sequential model with four or five increasing

lifetimes, i.e., $1 \rightarrow 2 \rightarrow 3 \rightarrow 4 \rightarrow 5$ (13, 16, 22). The species-associated difference spectrum (SADS) from this analysis summarize the spectral evolution. For example, the third SADS is formed from the second SADS with a lifetime τ_2 and decays with τ_3 ; thus, it dominates the real spectral data at times around τ_3 . At intermediate times between τ_2 and τ_3 , where the second SADS has partly decayed into the third SADS, the delta absorbance spectra are linear combinations of the two successive SADS. The first SADS represents the spectrum at time zero, and the last SADS represents the end spectrum. We note that for a target analysis of the data, which could lead to the right kinetic scheme to describe this complex system including reversible and branching reactions, more kinetic and energetic information is necessary. For that reason, we will base our first description of the radical pairs involved in electron transfer following 799 nm excitation on the time evolution of the spectra shown in Figures 2 and 3. It should, however, be noted that the SADS resulting from this analysis represent mixtures of the true states and that the lifetimes are a complicated function of the intrinsic rate constants. The function of the global analysis in this work is to use a simple kinetic scheme to throw further light upon the identity of the radical pairs involved in the alternative pathway(s) that Figure 2 clearly shows are operating in the YM210W mutant. The global analysis also gives an indication of the timescale over which these processes are occurring.

SADS are shown in Figure 3A–E for 880 nm excitation and in Figure 3F–K for 799 nm excitation. Only slow

charge separation from P^* is observed in Figure 2 on direct excitation of P with 880 nm pulses, this being reflected in the global analysis by two components of 80 ps and 500 ps (Figure 3B and Figure 3C). Since P^* -stimulated emission is observed in all SADS, except for the end spectrum (Figure 3D), it can be concluded that P^* is in equilibrium with the charge-separated states formed. The 80 ps component describes a process in which P^* partly decays and an electrochromic bandshift characteristic for $P^+H_A^-$ formation is formed (Figure 3C). It should be noted that simultaneous analysis over different wavelength windows and addition of the $P^+Q_A^-$ end spectrum (see Materials and Methods) were necessary to reveal this kinetic component. For some combinations of datasets, the rate constant of this process varied by up to 2 times the standard error of 20 ps. The spectrum of this species, however, hardly differed between the different analyses. The difficulty in revealing this component can be explained by the fact that the formation of $P^+H_A^-$ from P^* is slower than the decay from $P^+H_A^-$ to $P^+Q_A^-$. Therefore, the contribution of $P^+H_A^-$ is rather small in this mutant in all of the time-gated spectra. The 500 ps component reflects further decay of P^* and the development of the electrochromic bandshift signal that is characteristic for the formation of the $P^+Q_A^-$ radical pair. On a faster time scale, we also see a 2.5 ps process involving a blue shift or loss of stimulated emission in the 890–950 nm region, and a decrease of the positive feature at about 808 nm (Figure 3A,B). This process may be attributed to evolution of P^* into a state with more charge transfer character (18–20). An overlay of spectra 3A–D, showing the evolution of the system following 880 nm excitation, is given in Figure 3E.

Excitation of the YM210W RC at 799 nm results in the formation of B^* , which represents a mixture of predominantly B_A^* and some B_B^* and is manifested by a bleach at approximately 804 nm (Figure 3F). In this bleaching signal, both ground state bleaching and stimulated emission are present. B^* then undergoes a rapid (~ 200 fs) evolution into a state that has a lifetime of 6.5 ps. The state formed after 200 fs is characterized by a bleaching of the blue side of the B absorption band at 802 nm, a bleach of the P band, and a bleach in the H region at 753 nm (Figure 3G and Figure 2, solid spectrum at 1.3 ps). Superimposed on the bleached absorbance band at 802 nm, the small absorbance increase characteristic for P^* at 808 nm is observed. In Figure 4, we compare the SADS spectrum from Figure 3G with the inverted ground state absorbance spectrum at 77 K. The spectra are normalized on the blue side of the P absorbance band. The comparison shows that the persistent bleach in the SADS at 802 nm is blue-shifted from and narrower than the B absorption band, and can be assigned to the disappearance of the ground state absorption of B_A due to the formation of either B_A^+ or B_A^- . The ground state absorbance band of P also bleaches in spectrum G in Figure 3. This bleach contains a much smaller contribution from P^* -stimulated emission than is found when P is excited directly (Figure 3G compared with Figure 3A; this difference is also clearly seen in the data shown in Figure 2). This demonstrates that part of the bleach of the P ground state band following 799 nm excitation arises not from the formation of P^* , but rather from another state involving P, most likely P^+ . The bleach in the H absorption region in spectrum G is small and is mixed with other spectral components, in

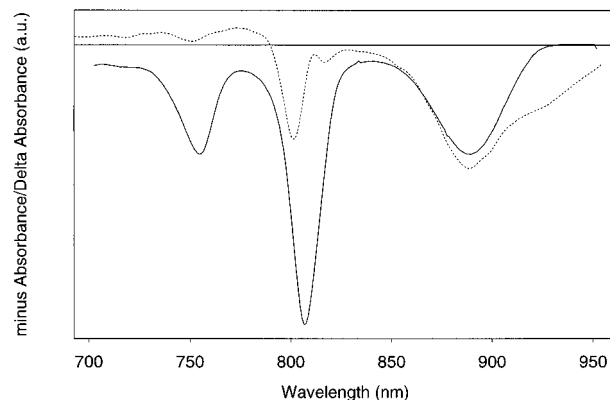


FIGURE 4: Comparison of the inverted ground state absorbance spectrum of membrane-bound YM210W RCs (solid line) and the SADS of the species formed from B^* with a lifetime of 200 fs (dotted line, Figure 3G). The spectra are normalized on the blue side of the P absorbance band and P bleaching signal, respectively.

particular the P^* excited state absorption, which makes it difficult to assign this feature to either H_A or H_B . It is also possible that this feature has another origin, for example, a small electrochromic bandshift of H_A absorbance caused by the presence of B_A^- . The early charge-separated state shown in Figure 3G then evolves with a time constant of 6.5 ps into a state with the spectroscopic characteristics of the $P^+H_A^-$ radical pair (Figure 3H, see also the solid spectra at 5, 9, and 17 ps in Figure 2). This 6.5 ps time constant also reflects an increase of the bleaching of P in the P absorption region, although the amount of P^* -stimulated emission does not increase. This suggests additional bleaching of the P ground state absorbance band, perhaps through the formation of P^+ following electron transfer from P to B_A^+ , i.e., the reaction $PB_A^+H_A^- \rightarrow P^+B_AH_A^-$. Figure 3K shows an overlay of spectra F–J.

We conclude from the data in which the RCs were excited at 799 nm that a charge-separated state is formed from B_A^* which in turn gives rise to efficient $P^+H_A^-$ formation. This intermediate state involves a bleaching of the B_A absorbance band. At least two more pigments contribute to this state; one is P^+ , and the second is a component other than P. In principle, direct charge separation from the excited state B_A^* could lead to the formation of the radical pairs $P^+B_A^-$ or $B_A^+H_A^-$. As we see a strong bleaching of B_A and P and a small bleaching of the H absorption band in the state that evolves from B_A^* (see the solid 1.3 ps spectrum in Figure 2, spectrum 3G in Figure 3, and Figure 4), it seems that the product of the subpicosecond electron transfer from B_A^* is a mixture of these radical pairs, or that a more complex description is appropriate (see below). Experiments are in progress in spectral regions where the different pigments can be detected more selectively to further solve the initial steps of the alternative electron transfer mechanism. Electron transfer from H_A^- to Q_A is reflected in the time constant of 30 ps and is associated with a red shift of the electrochromic shift of the B absorbance band and partial formation of the electrochromic shift of the H absorbance band that is characteristic for the state $P^+Q_A^-$. No significant changes in the P band region are associated with this lifetime. The slowest lifetime in the global analysis of the data is 400 ps and describes a process in which a relatively small amount of P^* that is formed decays to $P^+Q_A^-$. This P^* has been formed by energy transfer from the fraction of B_B^* (8) that is created by the 799 nm excitation pulse and by energy

transfer from B_A^* that competes with direct charge separation. The resulting 400 ps process observed here is identical to the dominant 500 ps process seen on direct excitation of P.

For the reasons outlined above, the data in Figures 2 and 3 lead us to the conclusions that two alternative pathways for charge separation may be operating in YM210W RC. These have the form of $PB_A^*H_A \rightarrow P^+B_A^-H_A$ and $PB_A^*H_A \rightarrow PB_A^+H_A^-$. The first of these schemes produces part of the bleach of the P band seen in the SADS of the 6.5 ps lifetime species (Figure 3G). The second scheme is indicated by the bleach of the H absorption band that is seen superimposed on the P^* excited absorbance in Figure 3G and the additional bleach of the P band that evolves from this state with a lifetime of 6.5 ps (Figure 3H), which is attributed to transfer of the electron hole from B_A^+ to P. The data in Figure 4 allow us to make a rough estimate of the efficiency of these proposed alternative pathways of charge separation. Figure 4 compares the SADS of the state that is formed in 200 fs from B_A^* with the ground state absorbance spectrum, normalized on the blue side of the P absorbance band where there is no contribution from stimulated emission. We assume that the bleach of the B band seen in the SADS arises from either B_A^+ or B_A^- in the two pathways described above, and that B_A contributes 50% to the area of the B absorbance band. From the comparison in Figure 4, it can be seen that 25% of the B absorbance band is bleached after the 200 fs process, which equates to 50% of the B_A band. However, this value is an overestimate as a comparison of Figure 3H with Figure 3G reveals that the bleaching of the P band has only reached $\sim 86\%$ of its maximal extent in the SADS of this 6.5 ps lifetime component. Therefore, the percentage bleaching of B_A is closer to $50\% \times 86\% = 43\%$, leading to the conclusion that 57% of the B^* formed passes its energy to P, driving conventional slow electron transfer, while 43% directly drives the alternative pathways of electron transfer with lifetimes on the order of 200 fs. If we further assume that the additional bleaching of the P band (14% of the overall total) seen following the 6.5 ps decay (Figure 3H, cf. Figure 3G) does represent the reaction $PB_A^+H_A^- \rightarrow P^+B_AH_A^-$, then we assign a yield of 14% of the overall formation of P^+ to the alternative pathway $PB_A^*H_A \rightarrow P^*B_A^+H_A^-$, leaving 29% of the charge separation in the system to the route $PB_A^*H_A \rightarrow P^+B_A^-H_A$. Put another way, of the 43% of the total RCs performing charge separation via the alternative pathway, one-third conducts the reaction via $PB_A^+H_A^-$ while two-thirds proceeds via $P^+B_A^-H_A$. Although this estimate only represents a rough approximation, it serves as a useful purpose in providing an indication of the efficiency of the direct route of charge separation relative to energy transfer to P. Finally, it should be noted that the part of B_B which is excited by the 799 nm excitation pulse probably has a 100% yield of energy transfer to P (7). Therefore, the relative efficiency of the alternative pathways starting from exclusively B_A^* will be higher than the 43% estimated in our calculations above.

Conclusions. Our results show unequivocally that at least one alternative pathway for charge separation can be demonstrated in *Rb. sphaeroides* RCs in addition to the heavily-studied reaction driven by P^* . In the YM210W mutant, the alternative pathway has a high yield, occurs on a subpicosecond time scale, and competes successfully with energy transfer from B_A^* to P. Our work demonstrates that

the excited states of the bacterial reaction center have unexpected dynamic properties that certainly require a variety of new experiments combined with new theory to be fully characterized. In support of our findings, we note that a route of electron transfer involving radical pair states such as $B_A^+H_A^-$ has been proposed previously on the basis of molecular calculations (23–25). It would seem from our results that there are some latent possibilities for light-driven transmembrane electron transfer in the bacterial RC that can be revealed and/or developed through site-directed mutagenesis. It may be possible that this (these) alternative pathway(s) also operate(s) in wild-type RCs at room temperature. In a recent study, the time-resolved difference spectra of WT RCs of *Rhodobacter sphaeroides* were measured as a function of excitation wavelength (26). Notable differences were observed in the evolution of the excited state on a subpicosecond time scale, with the relative amount of P^* formed after 1 ps depending on the excitation wavelength. In particular, 800 and 760 nm excitation yielded 15–20% less P^* than direct excitation of P. Although the authors of ref 26 did not arrive at a firm conclusion concerning the origin of this phenomenon, they discussed the possibility of direct charge separation from B_A^* as one explanation. Our experiments may be consistent with a significant yield of charge separation from B_A^* at room temperature in WT RCs, since we do not expect that the energy transfer or the rate of electron transfer from B_A^* is very dependent on temperature, although other changes associated with the YM210W mutation may have made the alternative pathway more efficient in the YM210W mutant.

To close, in addition to exhibiting the versatility of the bacterial RC, our findings may also have implications for the mechanism of charge separation in the oxygen-evolving photosystem II RC of higher plants. In this complex, it is likely that a multimer of weakly coupled pigments is a more appropriate description for the primary donor of electrons, rather than a chlorophyll dimer (27). The results presented here clearly show that the species that drives transmembrane electron transfer in photosynthesis does not necessarily have to be the excited state of a pigment dimer, nor does it have to be located at the periplasmic 'end' of the transmembrane chain of redox cofactors.

REFERENCES

1. Woodbury, N. W., and Allen, J. P. (1995) in *Anoxygenic Photosynthetic Bacteria* (Blankenship, R. E., and Bauer, C. E., Eds.) p 527, Kluwer Academic Publishers, Dordrecht, The Netherlands.
2. Parson, W. W. (1991) In *Chlorophylls* (Scheer, H., Ed.) p 1153, CRC Press, Boca Raton, FL.
3. Fleming, G. R., and Van Grondelle, R. (1994) *Phys. Today* 47, 48.
4. Breton, J., Martin, J.-L., Petrich, J., Migus, A., Antonetti, A., and Orszag, A. (1986) *Proc. Natl. Acad. Sci. U.S.A.* 83, 5121.
5. Stanley, R. J., King, B., and Boxer, S. G. (1996) *J. Phys. Chem.* 100, 12052.
6. Jonas, D. M., Lang, M. J., Nagasawa, Y., Joo, T., and Fleming, G. R. (1996) *J. Phys. Chem.* 100, 12660.
7. Van Brederode, M. E., Jones, M. R., and Van Grondelle, R., (1997) *Chem. Phys. Lett* 268, 143.
8. Van Brederode, M. E., Beekman, L. M. P., Kuciasukas, D., Jones, M. R., Van Stokkum, I. H. M., and Van Grondelle, R. (1996) in *The Reaction Center of Photosynthetic Bacteria* (Michel-Beyerle, M. E., Ed.) p 225, Springer, Berlin-Heidelberg.

9. Fleming, G. R., Martin, J.-L., and Breton, J. (1988) *Nature* 333, 190.
10. Parson, W. W., Chu, Z.-T., and Warshel, A. (1990) *Biochim. Biophys. Acta* 1012, 251.
11. Hamm, P., Gray, K. A., Oesterhelt, D., Feick, R., Scheer, H., and Zinth, W. (1993) *Biochim. Biophys. Acta* 1142, 99.
12. Jia, Y., DiMagno, T. J., Chan, C.-K., Wang, Z., Du, M., Hanson, D. K., Schiffer, M., Norris, J. R., Fleming, G. R., and Popov, M. P. (1993) *J. Phys. Chem.* 97, 13180.
13. Nagarajan, V., Parson, W. W., Davis, D., and Schenck, C. C. (1993) *Biochemistry* 32, 12324.
14. Shochat, S., Arlt, T., Francke, C., Gast, P., Van Noort, P. I., Otte, S. C. M., Schelvis, H. P. M., Schmidt, S., Vijgenboom, E., Vrieze, J., Zinth, W., and Hoff, A. J. (1994) *Photosynth. Res.* 40, 55.
15. Vos, M. H., Jones, M. R., Breton, J., Lambry, J.-C., and Martin, J.-L. (1996) *Biochemistry* 35, 2687.
16. Beekman, L. M. P., Van Stokkum, I. H. M., Monshouwer, R., Rijnders, A. J., McGlynn, P., Visschers, R. W., Jones, M. R., and Van Grondelle, R. (1996) *J. Phys. Chem.* 100, 7256.
17. Alden, R. G., Parson, W. W., Chu, Z. T., and Warshel, A. (1996) *J. Phys. Chem.* 100, 16761.
18. Woodbury, N. W., Lin, S., Lin, X., Peloquin, J. M., Taguchi, A. K. W., Williams, J., and Allen, J. P. (1995) *Chem. Phys.* 197, 405.
19. McDowell, L. M., Kirmaier, C., and Holten, D. (1990) *Biochim. Biophys. Acta* 1020, 239.
20. Hamm, P., and Zinth, W. (1995) *J. Phys. Chem.* 99, 13537.
21. Visser, H. M., Groot, M.-L., Van Mourik, F., Van Stokkum, I. H. M., Dekker, J. P., and Van Grondelle, R. (1995) *J. Phys. Chem.* 99, 15304.
22. Van Stokkum, I. H. M., Scherer, T., Brouwer, A. M., and Verhoeven, J. W. (1993) *J. Phys. Chem.* 98, 852.
23. Fischer, S. F., and Scherer, P. O. J. (1987) *Chem. Phys.* 115, 151.
24. Warshel, A., Creighton, S., and Parson, W. W. (1988) *J. Phys. Chem.* 92, 2696.
25. Alden, R. G., Hayashi, M., Allen, J. P., Woodbury, N. W., Murchinson, H., and Lin, S. H. (1993) *Chem. Phys. Lett.* 208, 350.
26. Lin, S., Taguchi, A. K. W., and Woodbury, N. W. (1996) *J. Phys. Chem.* 100, 17067.
27. Durrant, J. R., Klug, D. R., Kwa, S. L. S., Van Grondelle, R., Porter, G., and Dekker, J. P. (1995) *Proc. Natl. Acad. Sci. U.S.A.* 92, 4798.
28. Allen, J. P., Feher, G., Yeates, T. O., Komiya, H., and Rees, D. C. (1987) *Proc. Natl. Acad. Sci. U.S.A.* 84, 5730.
29. Ermler, U., Michel, H., and Schiffer, M. J. (1994) *Bioenerg. Biomembr.* 26, 5.
30. Jones, M. R., Visschers, R. W., Van Grondelle, R., and Hunter, C. N. (1992) *Biochemistry* 31, 4458.
31. Jones, M. R., Heer-Dawson, M., Mattioli, T. A., Hunter, C. N., and Robert, B. (1994) *FEBS Lett.* 339, 18.

BI9703756